Effect of impinging velocity on the erosive wear behaviour of polyamides

J. John Rajesh[a], J. Bijwe[a]*, B. Venkataraman[b], U.S. Tewari[a]

[a] *Industrial Tribology Machine Dynamics and Maintenance Engineering Centre, Indian Institute of Technology, Hauz Khas, New Delhi, 110 016 India*

[h] *Defence Metallurgical Research Laboratory, Hyderabad, India*

Received 28 September 2001; received in revised form 31 December 2002; accepted 30 March 2003

Abstract

Various parameters, such as type, size and velocity of erodent and impact angle, are important for the erosive wear behaviour of materials. In this work, the erosive wear behaviour of various polyamides (PAs), viz. PA 6, PA 66, PA 66/610, PA 11, PA 12 and aromatic PA with difference in the methylene to amide (CH_2/CONH) ratio in the backbone, was evaluated at two impact angles (30° and 90°) and at two impact velocities (80 and 140 m/s) using silica sand as erodent. The influence of impact velocity on erosion rate was more dramatic at an oblique impact angle (30°) than at normal impact angle (90°). Microscopic analysis of the eroded samples revealed that brittle fracture was the principal mode of failure in all the PAs at the normal impact. At the oblique impact, on the other hand, chipping off of material by microcutting and severe plastic deformation were observed.

Keywords: Polyamides; Erosive wear; Impinging velocity; Normal and oblique impacts

1. Introduction

Erosive wear of materials occurs by the removal of target material from the impact zone, due to repeated impacts of the erodent, by a micromechanical deformation/fracture process. In general, localized plastic flow is the principal mode of failure for ductile materials, whereas for brittle materials it is microcracking and chipping off of the materials. Polymers are increasingly being used for various applications such as helicopter rotor blades, radomes, etc., where erosion is inevitable. Though much work has been reported on the erosive wear behaviour of metals [1-4], comparatively less has been reported on the erosive wear performance of polymers and composites.

In general, the erosive wear behaviour of material depends on various operating parameters, such as velocity and angle of impact, particle size, shape, flux rate, etc. [2]. Literature on the effect of velocity of erodent on wear performance is sparse as compared to that on other parameters [5-9]. Earlier studies have shown that the value of the velocity exponent depends on the nature of both the target and the erodent. Tilly and Sage [10] reported a value of velocity exponent of 2.3 for 125—150 |jm quartz erodent impacting a range of materials from metals to plastics. They also reported that the velocity exponent decreased with decreasing size of the erodent. In contrast, Finnie [3] reported a high velocity exponent of 6.5 for 575 |jm steel spheres impacting glass. While studying the erosive wear behaviour of glass eroded by 300 |jm size iron spheres, Bitter [11,12] postulated that there was a threshold velocity value below which deformation was elastic and hence no damage occurred. Tilly [13] proposed that the threshold velocity depended on the particle size of the erodent and obtained a value of 2.7 m/s for 225 |jm quartz against 11% chromium steel. Wiederhorn et al. [14] documented the velocity exponents for seven types of target materials having a wide range of brittleness indices and microstructures. Scattergood and Routbort [15] found that the velocity exponent increased with decreasing particle size

of the erodent. While studying the erosive wear behaviour of amorphous polystyrene, Thai et al. [16] found that the velocity exponent was 3.69. Karasek et al. [17] observed almost linear correlation between the erosion rate of graphite fibre reinforced bismaleimide composite and the impinging velocity. Arnold and Hutchings [5] found that the erosion rate of natural rubber and epoxidized natural rubber had very strong dependence on the impinging velocity above 70 m/s. Rao et al. [18] reviewed the effect of impact velocity on the erosive wear of various polymers and composites. In our earlier work [19], the influence of impact angle and dose of the erodent on the erosive wear behaviour of various PAs with different methylene to amide (CH_2/CONH) ratio was investigated. Moreover, this ratio has significant influence on the thermo-mechanical properties of PAs [20] and hence on tribo-behaviour. Therefore, it was thought worthwhile to study the influence of impinging velocity of the erodent on the erosive wear behaviour of these PAs.

2. Experimental

2.1. Materials selected

Seven polyamides with the following chemical structures were procured in the form of granules.

PA 6: $(-NH-(CH_2)_5-CO-)_n$
PA 11: $(-NH-(CH_2)_{10}-CO-)_n$
PA 12[1]: $(-NH-(CH_2)_11-CO-)_n$
PA 66: $(-NH-(CH_2)_6-NH-CO-(CH_2)_4-CO-)_n$
PA 66/610: $(-NH-(CH_2)_6-NH-CO-(CH_2)_4-CO)_n-(NH-(CH_2)_6-NH-CO-(CH_2)_8-CO-)_m$
Aromatic PA[2]: (Amorphous copolyamide with aromatic, aliphatic and cyclo-aliphatic groups)

Prior to injection moulding, they were dried in a vacuum oven at 80 °C for 12 h. Sheets (200 mm x 200 mm x 6 mm) of these PA 6 and PA 12 were compression moulded by heating the granular materials placed in the mould at 270 and 215 °C, respectively, for an hour. Pressure (5 MPa) was then applied for one hour, with intermittent bumping to release trapped moisture, if any. Test bars as per ASTM standards were moulded and their mechanical properties were evaluated. The data along with other details are presented in Table 1. For erosive wear studies, dried granules of materials were compression moulded into sheets of 150 mm x 150 mm x 6 mm size. From these sheets, test samples of 30 mm X 30 mm X 6 mm size were cut for erosion wear studies.

2.2. Erosive wear studies

The solid particle erosion experiments were carried out using silica sand (90-180 |jm size) as the impinging particles. Dried and compressed air at two pressures (0.2 and 0.4 MPa) was allowed to mix with the silica sand, which was fed constantly, i.e. 4 g/min, by a conveyor-belt-type feeder in the mixing chamber. These fluidized silica sand particles were accelerated by passing them through a tungsten carbide converging nozzle of 6 mm diameter to bombard the polymer target (30 mm x 30 mm x 6 mm) held at a specific angle with respect to the flow of the impinging particles. The distance between the target material and the nozzle was approximately 10 mm. The impact velocities of the erodent particles were 80 and 140 m/s, and they were determined experimentally using the rotating double disc method developed by Ives and Ruff [21]. Erosive wear studies were done at two impingement angles (30° and 90°). Scanning electron microscopic (SEM) studies on eroded surfaces (after silver sputtering) were carried out on a Jeol JSM-840 scanning electron microscope to investigate the erosion mechanism.

3. Results and discussion

Erosive wear rate as a function of mass of erodent for PAs at 30° and 90° and at two impinging velocities is plotted as histograms in Figs. 1 and 2. Scanning electron micrographs of the eroded surfaces of PAs at 30° and 90° and at two velocities are shown in Figs. 3-5. The following are the salient features of the studies:

- Surface blackening at the impact zone was observed for all the materials at normal impact and at both the impact velocities.
- The order of performance of the materials at the two impact velocities and at the two impact angles was as follows:

  At α = 30°and v = 80 m/s: F > B>A≈D > G>E > C
  At α = 30° and v = 140 m/s: B > F>D > A>G > E>C
  At α = 90°and v = 80 m/s: D > B≈F > C>A > E>G
  At α = 90° and v = 140 m/s: F > B>D > C>A > E>G
- Though the same amount of erodent was used in every test for both velocity experiments, sand particles with higher energy (due to high velocity) damaged the polymer surface more severely. However,

[1] PA 12 was of two types. One was general purpose nucleated PA 12 and the other was medium viscosity extruded.
[2] The exact chemical structure was not available.

Table 1
Details of the selected materials

Property	PA 6	PA 11	PA 12 (L 16 GM)	PA 12 (L 20)	PA 66	PA 66/610 (BM 20SBG)	Aromatic PA+
Designation	A	B	C	D	E	F	G
Manufacturer	Du Pont India Ltd.	Elf Ato Chem, France	EMS Chemie, Switzerland	EMS Chemie, Switzerland	Du Pont India Ltd.	EMS Chemie, Switzerland	Elf Ato Chem, France
Trade name	Zytel	Rilsan	Grilamid LI6 GM	Grilamid L20	Zytel	Grilon BM20 SBG	Cristamid
Specific gravity	1.15	1.05	1.01	1.01	1.14	1.09	1.12
Tensile strength (MPa) ASTM D 638	58	48	36	37	42	31	57
Elongation to break (%)	325	393	173	282	207	100	30
Flexural modulus (MPa) ASTM D 790	59	12	29	37	64	31	51
Notched impact strength (kgm/m) ASTM D 256	4.92	5.90	5.90	10.82	3.93	5.90	1.96
Shore D hardness	74	66	79	76	80	76	85
Glass transition temperature[a] T_g (°C)	50	46	46	46	57	-	45
Melting temperature T_m (°C)	222	179	177	178	258	200	230
Degradation temperature[b] T_d (°C)	440	440	450	455	430	460	410

[a] This was the only PA that was amorphous, brittle, transparent and hard, with an aromatic group.
[b] Data extracted from TGA curves based on thermo-gravimetric analysis done on the samples.

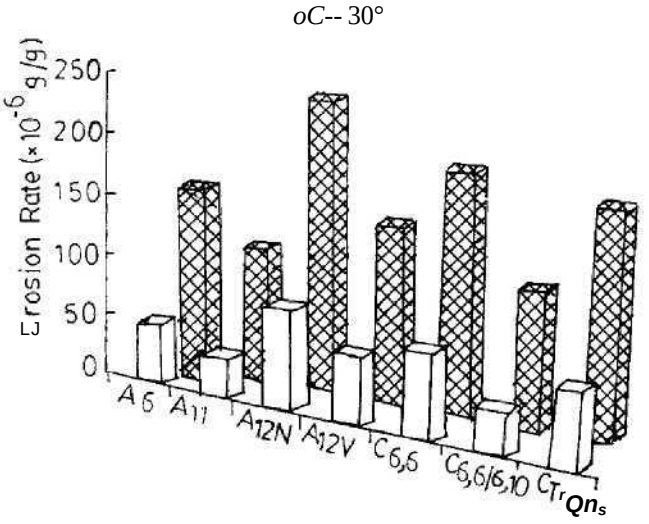

Fig. 1. Histogram showing the steady state erosive wear rates of all the materials at two impact velocities (i.e. at 80 and 140 m/s) for 30° impact. Unfilled, lower impact velocity and filled, higher impact velocity.

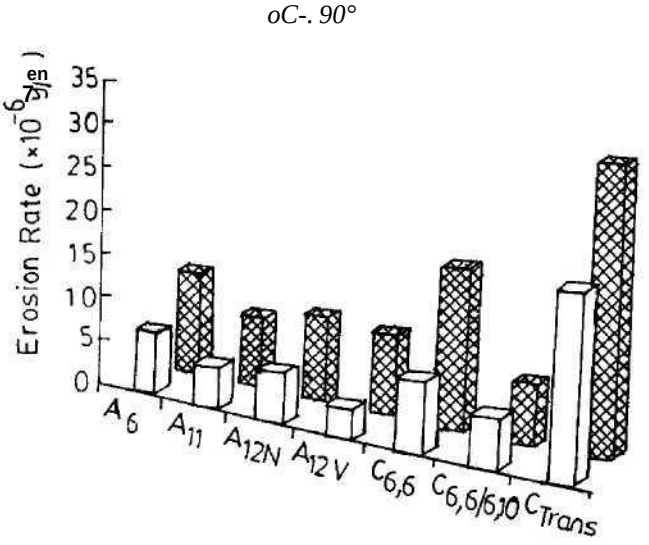

Fig. 2. Histogram showing the steady state erosive wear rates of all the materials at two impact velocities (i.e. at 80 and 140 m/s) for 90° impacts. Unfilled, lower impact velocity and filled, higher impact velocity.

the extent of damage depended on the material and angle of impact. The approximate extent of increase for all the materials is shown in Table 2.

- At normal impact and at lower impinging velocity (i.e. 80 m/s), a mass gain in the initial period was observed for all the materials except material G (material G was the only amorphous PA in the selected series of PAs). At higher impinging velocity (140 m/s), however, three materials, namely C, E and G, did not show initial mass gain.

In the initial stages of the normal impact, the erodent generally gets embedded on the surface of the target material (except for brittle material), and these embedded particles can act as stress concentration points from where, the microcracks can develop during successive impacts. In general, surface blackening was noticed at normal impact for both velocities. Owing to the poor thermal conductivity and stability of the polyamides, the incremental heat built up at the impact zone due to the repeated impacts led to the surface layer degradation of the target material [22]. However, no surface blackening was observed for the oblique impacts. According to Bulgin et al. [23], the tangential component of the impact force is largely responsible for erosion, and this varies approximately with the cosine of the angle of incidence. In the case of normal impact, the tangential component of the impact force is zero, whereas for the oblique impact (30°) it is =0.9 and hence leads to higher erosion rate. The erosion rates of all the PAs excluding material G decreased with increasing the dosage of erodent. However, the material G showed high erosion rate in the initial stage and later showed stabilization of the rate. Embedding was not possible in the case of this amorphous, hard and stiff polymer.

Investigations on the correlation between erosive wear rate and mechanical properties have been reported by many authors in the case of various polymers and metals [7,14]. In case of the PAs selected, erosive wear at the lower velocity (80 m/s) and two impact angles, viz. 60° and 90°, good correlation between brittleness index and erosive wear rate was observed [19]. For the higher velocity, however, no such relation with any combination of properties was observed. This could possibly be due to the fact that the mechanical properties, as seen in Table 1, are in static mode, while during erosion, due to dynamic strain rates of the order 10^4—10^5 per second, polymers, being visco-elastic materials and very sensitive to thermal changes, exhibit rate-sensitive flow and fracture behaviour. Hence, at higher velocity no correlation emerged between erosive wear rate and the mechanical properties.

Zahavi [8] investigated the erosive wear behaviour of polyurethane, elastomeric and fluorocarbon coatings and reported that the formation, propagation and intersection of microcracks were mainly responsible for the failure of the coatings. While investigating the erosive wear behaviour of natural rubber and epoxidized natural rubber at 30° and 90°, Arnold and Hutchings [5] concluded that the formation of fine fatigue cracks under tensile surface stresses was responsible for failure. Pool et al. [24] observed that continuous graphite fibre reinforced epoxy composite exhibited the brittle failure mechanism, while for continuous aramid fibre reinforced epoxy and chopped graphite fibre reinforced polyphenylene sulfide the quasi-ductile behaviour was the primary failure mechanism.

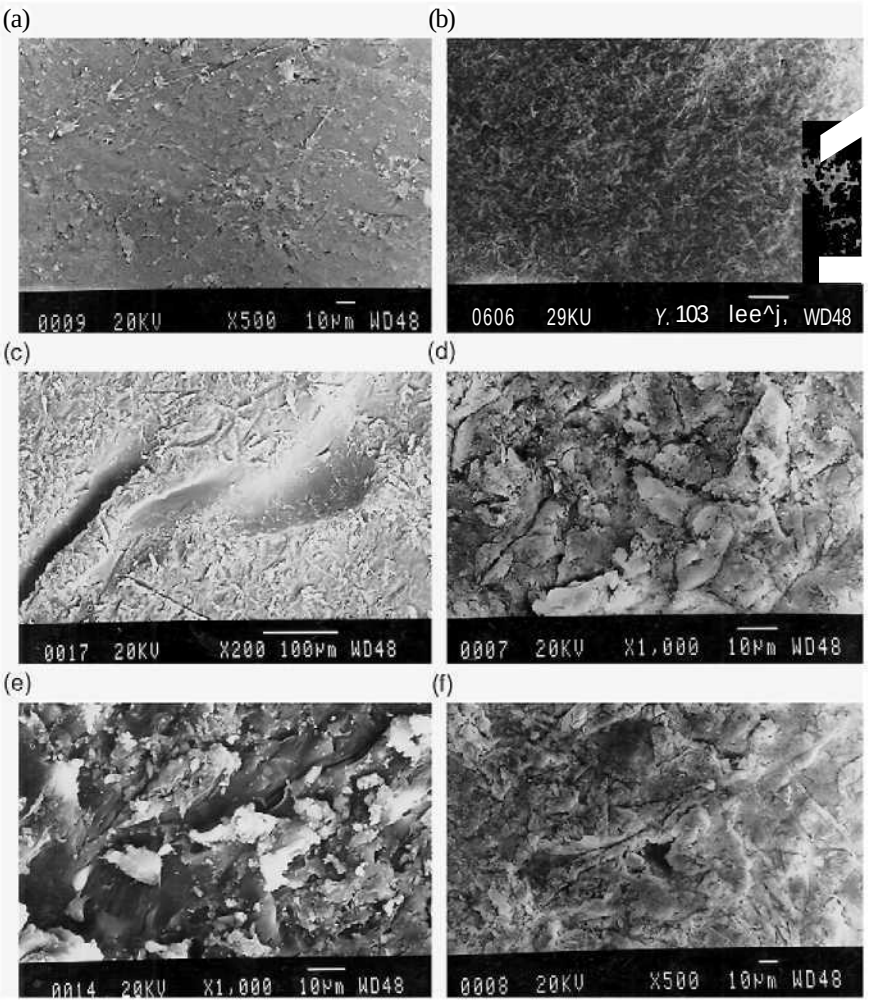

Fig. 3. SEM micrographs of eroded surfaces of PA 66/610 under different condition (a) surface farthest from the eroded zone; (b) and (c) α = 30° and v = 140 m/s; (d) and (e) α = 90° and v = 140 m/s; and (f) α = 90° and v = 80 m/s.

4. Microscopic analysis

Eroded surfaces of PA 66/610 under different operating conditions are shown in micrographs in Fig. 3. Micrograph 3 a shows the surfaces farthest from the eroded zone and indicates the general topography of the unaffected surface. Micrographs 3b and 3c are for the eroded surfaces of the crater (α = 30° and v = 140 m/s), while micrograph 3d shows the general appearance of the crater under low magnification (α = 90° and v = 140 m/s). Micrographs 3e and 3f shows the difference in surface topography because of velocity difference (3e $\boldsymbol{\alpha}$ = 90° and v = 140 m/s; 3f $\boldsymbol{\alpha}$ = 90° and v = 80 m/s). At 30° impact, both abrasion and erosion processes play important roles. The sand particles, after impacting, slide on the surface and abrade while dropping down. The wear and hence damage is more than that in the case of normal impact. Marks of material damage in the form of wide cracks and small craters (due to erosion) can be seen in micrograph 3b. Marks of microploughing of the ductile material in the form of elongated sheets from the furrows can also be seen in micrograph 3c. Change in impact angle from oblique to normal changes the topography of the damaged surface very significantly. Micrograph 3e (α = 90° and v = 140 m/s) shows the dominance of microchipping and microcracking phenomena. Multiple cracks originated from the point of impact and during this stress releasing process, and the cracks intersected and formed wear debris due to brittle fracture. After repetitive impacts, the debris in platelet form is removed and accounts for the measured wear loss. The drastic difference in surface damage due to ductile failure and plastic failure is clearly seen in micrograph 3c (α = 30° and v = 140 m/s) and 3d (α = 90° and v = 140 m/s). Differences in the topography of surfaces due to different impinging velocities can be seen in micrographs 3e (α = 90° and v = 140 m/s) and 3f ($\boldsymbol{\alpha}$ = 90° and v = 80 m/s). Since the impact angle is the same (α = 90°), the nature of failure (brittle) and appearance of the surface is almost identical, except for the extent and depth of microcracks. Overall, high velocity has rendered the surface more damaged, and high

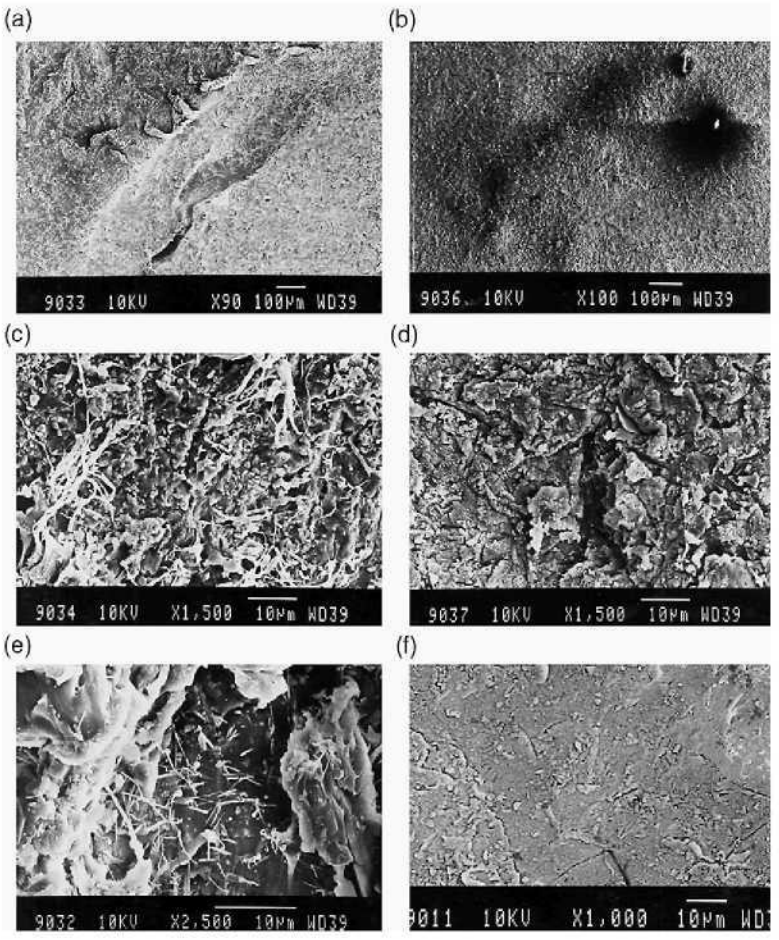

Fig. 4. SEM micrographs of eroded surfaces of PA 11 under different conditions (a), (b) and (c) a = 30° and v = 140 m/s; (d) and (e) a = 90° and v = 140 m/s; and (f) a = 90° and v = 80 m/s.

material removal and hence high wear is seen in the worn surface topography.

Worn surfaces of PA 11 under different operating conditions are shown in Fig. 4. Micrographs 4a, 4b and 4c are for eroded surfaces at oblique angle (v = 140 m/s) while 4d, 4e and 4f are for surfaces at normal impact (4d and 4c for v = 140 m/s; 4f for v = 80 m/s). The typical behaviour of abrasion along with erosion at a = 30° can be seen in micrograph 4a. This polymer has shown intermediate wear behaviour among the three PAs selected for microscopic analysis (wear resistance in order: PA 66/610 > PA 11 > Aromatic PA). Among the three PAs, PA 11 has shown the highest elongation to break (Table 1). This has reflected in the failure behaviour as well. An abundance of elongated fibres during the microploughing process is evident on the surface (4b and 4c). The probability and frequency of wear debris removal is less when ductile failure is the dominant wear mechanism. In the case of normal impact (4d, 4e and 4f), this failure mode was absent. Micrograph 4d shows a general view of the crater (a = 90° and v = 140 m/s), while the enlarged view shows the details of mode of failure. Plastic deformation and propagation of multiple cracks in all directions during the impact of high energy particles are the dominant mechanisms as discussed in micrographs 3e and 3f. Micrograph 4f shows the surface when the velocity was low. Overall, the damage and extent of cracks are significantly low in this case.

Micrographs of eroded surfaces of the aromatic PA have been collected in Fig. 5. Micrographs 5 a and 5b are for oblique impact (v = 140 m/s), while 5c is for normal impact (v = 140 m/s). Micrographs 5d, 5e and 5f are for oblique impact at a lower velocity (80 m/s). The typical behaviour of erosion along with abrasion is seen at oblique impact (5a and 5b). This aromatic PA was the only PA that was amorphous, transparent and very hard. It showed the highest wear, and its properties have reflected in the failure modes too. It showed the minimum value of elongation to break (Table 1). Though at a = 30°, abrasion is evident on the surface, no marks of ductile failure are present. On the contrary, this material has shown predominantly brittle failure. Another striking feature of the surface (5a, 5b and 5d) is the evidence of surface melting. Among the three PAs, this one has the highest melting point. However, the

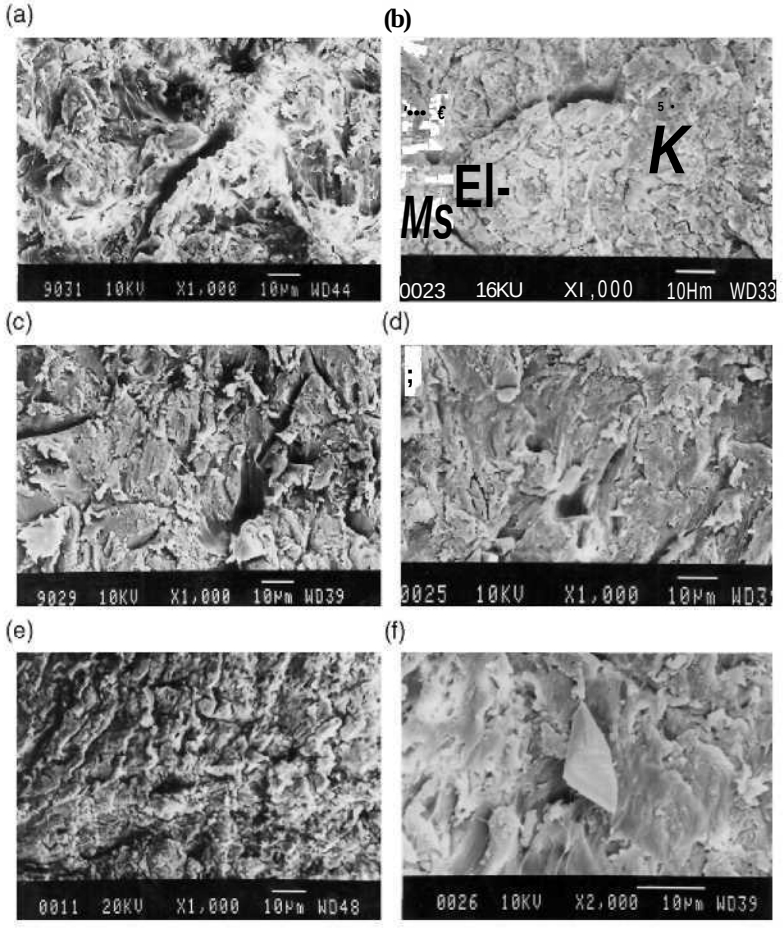

Fig. 5. SEM micrographs of eroded surfaces of aromatic PA under different condition: (a) and (b) *a* = 30° and v = 140 m/s; (c) *a* = 90° and v = 140 m/s; (d), (e) and (f) a = 30° and v = 80 m/s.

Table 2
Approximate percentage of increase in erosion rates (steady state) at two impact angles due to higher energy of particles at high velocity

Material	*a* = 30°	*a* = 90°
A	180	70
B	240	70
C	190	60
D	160	210
E	180	130
F	220	30
G	200	50

mode of energy dissipation being inefficient has led to melting of the surface. Such behaviour was not seen in the case of PA 11 (micrograph 4b), whose melting point is very low because of effective energy dissipation. Micrographs 5a and 5b, when compared to 5c, support the high wear of material when impacted at $a = 30°$. Very wide grooves and cracks are typical of a high extent of abrasion and erosion. Micrograph 5c is for normal impact topography and supports the observed lower wear. Multiple cracks indicate typical brittle failure under such impacting conditions. The difference in surface topography due to high energy impact (micrographs 5a and 5b for $a = 30°$ and v = 140 m/s) and low energy impact (micrographs 5d and 5f for $a = 30°$ and v = 80 m/s) explains the difference in wear behaviour. Overall, the features are the same, but the severity of damage is low in the case of low velocity.

5. Conclusion

Investigations were done on the erosive wear of seven different polyamides due to sand particle impingement with varying angle of impact and velocity. It was concluded that the same amount of particles when bombarded at higher velocity damaged the surface of polymers very significantly and resulted in excessively high wear. The extent of increase in wear, however, depended on the materials and the angle of impact. The velocity effect was more prominent at the oblique angle of impact. Scanning electron microscopic analysis confirmed the differences between the failure mechanisms at the oblique and normal impact and higher velocity and lower velocity as well.

Acknowledgements

The authors gratefully acknowledge the Council of Scientific and Industrial Research (CSIR), New Delhi, India, for the financial support and EMS Chemie, Switzerland, for supplying some polyamides to carry out this work.

References

[1] Levy AV. Solid particle erosion and erosion-corrosion of materials. Ohio (USA): ASM International, 1995.
[2] Tilly GP. Erosion caused by impact of solid particles. In: Scott D, editor. Treatise on materials science and technology, vol. 13. 1979. p. 28-7.
[3] Finnie I. Erosion of surfaces by solid particles. Wear 1960;3:87-103.
[4] Finnie I, McFadden DH. On the velocity dependence of the erosion of ductile metals by solid particles at low angles of incidence. Wear 1978;48(1):181-90.
[5] Arnold JC, Hutchings IM. The mechanisms of erosion of unfilled elastomers by solid particle impact. Wear 1990;138:33^6.
[6] Arnold JC, Hutchings IM. Flux rate effects in the erosive wear of elastomers. J Mater Sci 1989;24:833-9.
[7] Friedrich K. Erosive wear of polymer surfaces by steel ball blasting. J Mater Sci 1986;21:3317-32.
[8] Zahavi J. Solid particle erosion of polymeric coatings. Wear 1981;71:191-210.
[9] Williams Jr. JH, Lau KE. Solid particle erosion of graphite epoxy composites. Wear 1974;29:219-30.
[10] Tilly GP, Sage W. The interaction of particle and material behaviour in erosion processes. Wear 1970;16:447-65.
[11] Bitter JGA. A study of erosion phenomena, part 1. Wear 1963;6:5-21.
[12] Bitter JGA. A study of erosion phenomena, part II. Wear 1963;6:169-90.
[13] Tilly GP. A two stage mechanisms of ductile erosion. Wear 1973;23:87-96.
[14] Wiederhorn SM, Hockey BJ. Effect of material parameters on the erosion resistance of brittle materials. J Mater Sci 1983; 18:766-80.
[15] Scattergood RO, Routbort JL. Velocity and size dependence of the erosion rate in silicon. Wear 1981;67:227.
[16] Thai CM, Tsuda K, Hojo H. Erosion behaviour of polystyrene. J Test Eval 1981;9(6):359-65.
[17] Karasek KR, Goretta KC, Helberg DA, Rourbort JL. Erosion in bismaleimide polymers and bismaleimide-polymer composites. J Mater Sci Lett **1992;11:1143^4.**
[18] Rao PV, Buckley DH. Angular particle impingement studies of thermoplastic materials at normal incidence. ASLE Trans 1985;29(3):283-98.
[19] John Rajesh J, Bijwe J, Tewri US, Venkataramanan B. Erosive wear of various polyamides. Wear 2001;249(8):702-714
[20] Kohan MI. Nylon plastics handbook. Cincinnati (USA): Hanser/Gardner Publications Inc, 1995.
[21] Ruff AW, Ives LK. Wear 1975;35:195.
[22] Tilly GP. Erosion caused by airborne particles. Wear 1969; 14:63-79.
[23] Bulgin D, Walters MH. In: Proceedings of the International Rubber Conference. London (UK): MacLaren; 1967. p. 197-218.
[24] Pool KV, Dharan CKH, Finnie I. Erosive wear of composite materials. Wear 1986;107:1-12.